The magnetic phase transition and magnetocaloric effect in $Sm_{0.58}Sr_{0.42}MnO_3$ nanoparticles

The-Long Phan [a], T.D. Thanh [a,b], P. Zhang [a], D.S. Yang [c], S.C. Yu [a,*]

[a] Department of Physics, Chungbuk National University, Cheongju 361-763, South Korea
[b] Institute of Materials Science, Vietnam Academy of Science and Technology, Cau Giay, Hanoi, Vietnam
[c] Physics Division, School of Science Education, Chungbuk National University, Cheongju 361-763, South Korea

ARTICLE INFO

ABSTRACT

It is known that $Sm_{0.58}Sr_{0.42}MnO_3$ (SSMO) with a first-order magnetic phase transition exhibits colossal magnetoresistance and magnetocaloric effects around the Curie temperature (T_C). However, the effects just occur in a narrow temperature range due to the first-order nature. This work points out that its phase transition width and magnetocaloric effect is easily modified upon the fabrication of SSMO nanoparticles (NPs). Our detailed studies also demonstrate a clear tendency of the magnetic phase transformation from first to second order when the crystallite size (d) of NPs are reduced below 65 nm. Though the d decrease usually leads to the suppression of the T_C, magnetization, and magnetic-entropy change, the phase transition width is increased remarkably, thus widening the application range of SSMO. These interesting features are related to changes of the lattice strain, surface defect density, and electronic structure of Mn ions in NPs.

© 2013 Elsevier Ltd. All rights reserved.

Recently, narrow bandwidth perovskite-like manganites $R_{1-x}A_xMnO_3$ (R=Sm, Eu, Tb, Pr; A=Ca, Sr) have been of intensive interest because these compounds exhibit many unusual magneto-electronic properties around magnetic phase transitions [1–8]. Depending on A-doping concentration (x), crystal structure, and temperature, their magnetic properties can be paramagnetic (PM), ferromagnetic (FM), antiferromagnetic (AFM), and/or spin glassy [5–7]. These phenomena are arisen from strong interplay between spin, lattice, and orbital degrees of freedom, where both R and Mn ions can contribute magnetic interactions.

Among $R_{1-x}A_xMnO_3$ manganites, $Sm_{1-x}Sr_xMnO_3$ has attracted special interest [1,4,6,9–15]. Its magnetic phase diagram shown in detail by Tomoka and Kurbakov et al. is quite complicated [6,10]. In the Sr-doping range x=0.35–0.50, besides dominant FM inter-actions there is the presence of AFM interactions persisting above the Curie temperature (T_C) [1,4,6,10–12,15]. Particularly, their FM–PM phase transition around T_C is followed up with structural changes [6,16], and known as a first-order magnetic phase transi-tion (FOMT). This results in noticeable physical phenomena, such as colossal magnetoresistance, and giant magnetocaloric (MC) effects [1,4,9]. Due to the FOMT nature, however, the effects in $Sm_{1-x}Sr_xMnO_3$ (x=0.35–0.50) compounds only occur in a narrow temperature region. Their operating range for electronic devices (magnetic sensors, reading and recording heads, and so forth) in

CMR applications, and their refrigerant capacity (an important parameter in evaluating a MC material besides the magnetic entropy change) [17] in magnetic refrigeration applications are confined. Widening the phase transition width is thus necessary.

Experimentally, broadening the first-order transition region of $Sm_{1-x}Sr_xMnO_3$ (x=0.35–0.50) compounds can be carried out by applying a magnetic field $H > 40$ kOe, and hydrostatic pressure $P > 2.5$ GPa, or by fabricating low-dimensional systems. With these, a first-to-second order phase transformation takes place [8,11–15], reducing hysteretic losses, which is beneficial to the refrigerant capacity (RC) of magnetic refrigeration [18]. For appli-cation aspects, however, the use of $H > 40$ kOe is very difficult to deploy because conventional electronic devices only create magnetic-field magnitudes below 20 kOe. A similar challenge is also met if using high hydrostatic pressures [8]. Clearly, the alternative route of synthesizing low-dimensional materials is more feasible. Reviewing previous works, we realize that very few works were performed on $Sm_{0.5}Sr_{0.5}MnO_3$ nanoparticles and thin films prepared by the bottom-up approach [13–15]. Further-more, physical mechanisms related to variations of magnetic parameters (such as the T_C, saturation magnetization (M_s), absolute magnetic-entropy change ($|\Delta S_M|$), and so forth) in reduced dimensionality systems have not been clarified yet. In an attempt to light up this research direction, we have prepared $Sm_{0.58}Sr_{0.42}MnO_3$ (SSMO) nanoparticles (NPs) from a well-understood bulk sample with the FOMT [1,6,11,12] by using the mechanical milling (i.e., the top-down approach), and then studied their magnetic properties and MC effect. Our experimental results

* Corresponding author. Tel.: +82 43 261 2269; fax: +82 43 275 6416.
E-mail address: scyu@chungbuk.ac.kr (S.C. Yu).

reveal that by changing the averaged crystallite size (d) upon changing the milling time (t_m), the phase-transition width and MC effect can be easily modified. Although the d decrease causes the suppression of T_C, M_s, and $|\Delta S_M|$, the phase-transition width is increased remarkably. Based on detailed studies of X-ray diffraction (XRD) patterns and X-ray absorption spectra, we suggest that these phenomena are due to the changes related to the lattice strain, surface defects, and electronic structure of Mn ions in SSMO NPs.

To fabricate SSMO NPs, firstly a polycrystalline bulk sample with the FOMT was prepared by conventional solid-state reaction. Commercial high-purity powders (3N) of La_2O_3, CaO, $MnCO_3$, and Sm_2O_3 were combined in stoichiometrical quantities, and well mixed by using an agate mortar and pestle. The mixture was then pre-annealed at 1200 °C for 24 h. After several times of the pre-annealing and grinding, the mixture was pressed into a pellet, and annealed at 1300 °C for 48 h in air. The product obtained was ground in powder, and divided into parts of 1.5 g for the mechanical milling at different times of $t_m = 2$, 5, 8, 15, and 30 min (the initial/as-prepared bulk sample is denoted as $t_m = 0$), used the grinding medium of a zirconia vial (45 mL volume) and two balls ($\sim$13 mm diameter) supplied by SPEX-SamplePrep. The ball-to-powder mass ratio of 5.5 was fixed. Before milling, the coating was carefully made to minimize unexpected impurities generated from the vial and balls. In the final nanocrystalline products the crystal structure was checked by using an X-ray diffractometer (SIEMENS-D5000) with a radiation source of Cu-$K\alpha_1$ ($\lambda = 1.5406$ Å). Magnetic measurements versus temperature (with increments of 2–5 K) and external magnetic field (0–50 kOe) were performed on a superconducting quantum interference device magnetometer. Local geometric and electronic structures of SSMO NPs were investigated by X-ray absorption fine structure (XAFS) spectroscopy in the Pohang Accelerator Laboratory, South Korea. XAFS spectra in the transmission configuration were measured for the Mn K-edge (with $E_0 = 6539$ eV). For reference, absorption spectra of MnO_2, and Mn_2O_3 were also recorded.

With changing t_m as described above, we collected NPs with various crystallite sizes. XRD patterns recorded at room temperature proved the samples to be single phase in an orthorhombic structure (space group: $Pnma$) without the trace of secondary phases. The linewidth (β) of XRD peaks increases with increasing t_m. This is due to the d reduction, and the increase of the lattice strain (ε) and surface defect density. Having used the Williamson–Hall (W–H) equation $\beta \cos\theta = (K\lambda/d) + 2\varepsilon \sin\theta$, where $K = 0.9$ is the shape factor [19], we determined the average values of d and ε. As shown in Table 1, d decreases rapidly from 280 to 21 nm with increasing t_m from 0 to 30 min; notably, $d = 280$ nm is herein an estimated value for the $t_m = 0$ sample, its real value can be greater because the W–H method is more accurate for NPs with $d < 100$ nm. In contrast, the gradual reduction of d enhances ε from twice to about five times. Based on the XRD patterns, we also determined the lattice constants (a, b, c, and V), Table 1, in which V slightly increases with decreasing d. Such structural variations

generated from lowering the dimensionality influence directly magnetic properties of SSMO NPs.

Learning about this issue, we have investigated temperature and magnetic field dependences of magnetization. Fig. 1(a) and its inset show zero-field-cooled (ZFC) and field-cooled (FC) magnetizations versus temperature (denoted as $M_{ZFC}(T)$ and $M_{FC}(T)$, respectively) of SSMO NPs in a magnetic field (H) of 100 Oe. For the samples with $d = 280$ and 96 nm at temperatures $T > 40$ K, a gradual decrease in magnetization becomes rapid as raising temperature above 100 K due to the FM–PM phase transition, where FM coupling of magnetic moments is collapsed by thermal energy. Similar to SSMO bulk samples studied previously [1,6,11,12], the FM–PM phase transition followed by structural changes [6,16] is sharp with a width of 15–20 K, and belongs to the FOMT. If the temperature is lowered below 40 K, the reduction of magnetization obeys a power function $M(T) = c_1 + c_2 \times T^{3/2}$, where c_1 and c_2 are constants; in our case, $M_{ZFC}(T) \propto 0.032 \times T^{3/2}$ for $d = 290$ nm, and $M_{ZFC}(T) \propto 0.02 \times T^{3/2}$ for $d = 96$ nm. The $M_{ZFC}(T)$ curves of these two samples exhibit a sharp cusp at $\sim$40 K (named T_N) corresponding to an AFM–FM transition, where AFM order is assigned to Sm moments [11]. Its value is shifted about 2 K towards lower temperatures for the case of the $M_{FC}(T)$ curves. However, for the samples with $d = 65$, 52, 32 and 21 nm, see Fig. 1(a), their $M_{ZFC/FC}(T)$ curves have a bow-like shape, and exhibit some noticeable features: (i) the FM–PM transition width is broadened remarkably, about 80–100 K; (ii) the sharp cusp observed for the samples $d = 280$ and 96 nm at T_N is blurred and seems invisible; and (iii) the power law $T^{3/2}$ is not suitable to
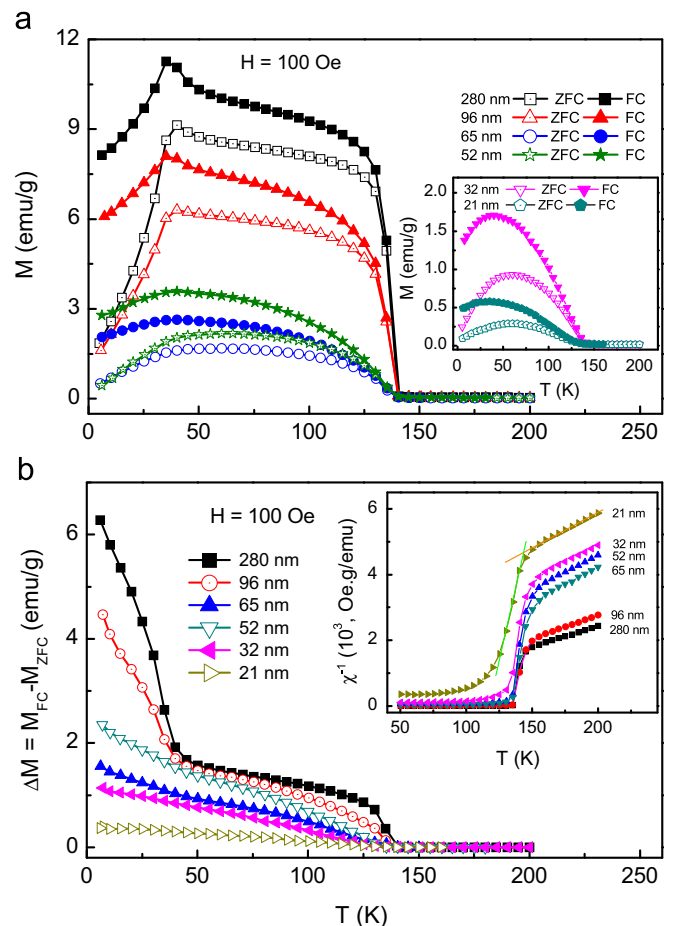

Table 1
Experimental parameters obtained for SSMO NPs; here, T_C obtained from $M(T)$ data with $H = 100$ Oe, and $|\Delta S_{max}|$ and RC values obtained for $\Delta H = 50$ kOe.

t_m (min)	d (nm)	ε	a (Å)	b (Å)	c (Å)	V (Å³)	T_C (K)	$|\Delta S_{max}|$ (J/kg K)	RC (J/kg)
0	280	0.005	5.491	5.433	7.669	228.78	135	9.3	302
2	96	0.006	5.491	5.433	7.670	228.82	135	5.9	208
5	65	0.012	5.492	5.433	7.669	228.83	133	2.3	85
8	52	0.016	5.492	5.433	7.669	228.83	133	3.1	132
15	32	0.021	5.492	5.432	7.671	228.85	128	1.2	78
30	21	0.027	5.493	5.432	7.671	228.88	118	0.5	45

Fig. 1. (a) $M_{ZFC/FC}(T)$ and (b) $\Delta M(T)$ curves for NPs with $d = 21$–280 nm in the field $H = 100$ Oe; The inset of (b) plots $\chi^{-1}(T)$ data in the FM and PM regions.